ADVANCED FUNCTIONAL MATERIALS
www.afm-journal.de

From Melamine-Cyanuric Acid Supramolecular Aggregates to Carbon Nitride Hollow Spheres

Young-Si Jun, Eun Zoo Lee, Xinchen Wang, Won Hi Hong, Galen D. Stucky, and Arne Thomas**

Graphitic carbon nitride (g-CN) is a promising heterogeneous metal-free catalyst for organic photosynthesis, solar energy conversion, and photodegradation of pollutants. Its catalytic performance is easily adjustable by modifying texture, optical, and electronic properties via nanocasting, doping, and copolymerization. However, simultaneous optimization has yet to be achieved. Here, a facile synthesis of mesoporous g-CN using molecular cooperative assembly between triazine molecules is reported. Flower-like, layered spherical aggregates of melamine cyanuric acid complex (MCA) are formed by precipitation from equimolecular mixtures in dimethyl sulfoxide (DMSO). Thermal polycondensation of MCA under nitrogen at 550 °C produces mesoporous hollow spheres comprised of tri-*s*-triazine based g-CN nanosheets (MCA-CN) with the composition of $C_3N_{4.14}H_{1.98}$. The layered structure succeeded from MCA induces stronger optical absorption, widens the bandgap by 0.16 eV, and increases the lifetime of photoexcited charge carriers by twice compared to that of the bulk g-CN, while the chemical structure remains similar to that of the bulk g-CN. As a result of these simultaneous modifications, the photodegradation kinetics of rhodamine B on the catalyst surface can be improved by 10 times.

1. Introduction

Molecular cooperative assembly is the spontaneous formation of stable aggregates formed by non-covalent bonds among molecules under equilibrium conditions. In particular, cooperative assembly structures have been prepared using intermolecular interactions such as hydrogen bonding, metal coordination and dipolar coupling with a variety of molecule-substrate systems. Hydrogen bonding is often exploited in the formation of supramolecular aggregates, as these non-covalent interactions have a strong directional component, which simplifies the design of complementary subunits for recognition and binding.[1] Several molecular motifs have been described to assemble into supramolecular structures, often based on melamine and cyanuric acid or derivatives therefrom.[2] One single melamine molecule can form three hydrogen bonds with cyanuric acid, yielding highly stable connections.

Melamine and other triazine derivatives are precursors for polymeric melon or graphitic carbon nitride (g-CN), a material that has recently gained increasing interest because of its catalytic and photocatalytic properties.[3–7] g-CN features a band structure (conduction band (CB) = –1.42 V, valence band (VB) = 1.28 V vs. Ag/AgCl at pH 6.8) straddling potentials of both water reduction and water oxidation.[7] The advantages of this metal-free photocatalyst are the low cost, the high chemical and thermal stability, and the possibility that simple inorganic or organic processing tools can be used to fine-tune the texture and photoelectric properties. Indeed, it has been shown that g-CN with high surface area and controlled nanostructures from nanoparticles to mesoporous materials[4,8] can be prepared by hard templating strategies using liquid precursors such as cyanamide.[9] The copolymerization of g-CN precursor with organic monomers like barbituric acid enables its optical absorption to cover more of the visible light.[10] These strategies not only improve the photocatalytic activity and selectivity of pristine g-CN, but they also pave the way for further modification of g-CN with sensitizers and co-catalysts. It is, however, still desirable to develop a new synthetic way concerning 1) fast charge recombination, 2) moderate water oxidation power, 3) low utilization of visible light, and 4) utilization of harmful hydrofluoric acid for the removal of hard template. Especially, a simple way to simultaneously address these issues and further improve texture and photoelectric properties of g-CN has yet to be achieved.

Of particular interest is that the combination of melamine with cyanuric acid as a precursor might add several advantages

Dr. Y.-S. Jun, Prof. G. D. Stucky
Department of Chemistry and Biochemistry
University of California
Santa Barbara, CA 93106, USA
Dr. E. Z. Lee, Prof. W. H. Hong
Department of Chemical and Biomolecular Engineering
Korea Advanced Institute of Science and Technology (KAIST)
373-1, Guseong-dong, Yuseong-gu, Daejeon 305-701, Korea
E-mail: whhong@kaist.ac.kr
Prof. X. C. Wang
Research Institute of Photocatalysis
State Key Laboratory Breeding Base of Photocatalysis
Fuzhou University, Fuzhou 350002, P. R. China
Prof. A. Thomas
Department of Chemistry/Functional Materials
Technische Universität Berlin
Hardenbergstr. 40, 10623 Berlin, Germany
E-mail: arne.thomas@tu-berlin.de

DOI: 10.1002/adfm.201203732

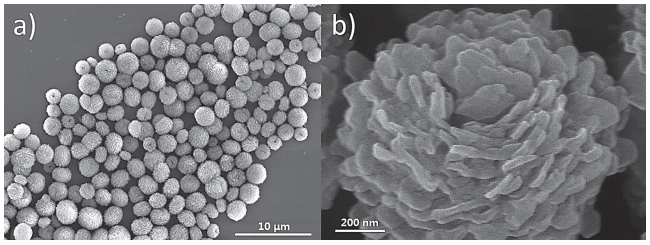

Figure 1. SEM images of MCA.

to the synthesis of g-CN for photocatalytic applications. 1) The molecular cooperative assembly can be expected to yield preformed micro- or nanostructures depending on the precursor molecules, solvent type, and synthesis temperatures, which might be incorporated into the subsequently formed carbon nitride. 2) The use of unsaturated cyanuric acid or preformed molecular cooperative assembly as a precursor might also modify the polycondensation and the chemical structure of g-CN with the formation of a band structure that would facilitate electron transfer and delocalization. Herein, we demonstrate that the simple molecular cooperative assembly of cheap triazine molecules is a unique precursor material enabling simultaneous optimization of the texture and photoelectric properties of g-CN. Formation and polycondensation of melamine cyanuric acid complex (MCA) are described. The resulting MCA-CN is characterized in terms of chemical structure, morphology, optical and electronic properties. The photocatalytic activity under visible light is also examined using the degradation of rhodamine B (RhB), a common organic substance used for this purpose.

2. Results and Discussion

2.1. Formation of Molecular Cooperative Assembly between Melamine and Cyanuric Acid

Molecular, hydrogen-bonded supramolecular aggregates have been formed by precipitation from equimolecular mixtures of melamine and cyanuric acid in dimethyl sulfoxide (DMSO). Melamine and cyanuric acid are insoluble in most solvents, but both are soluble in DMSO. Therefore, both compounds were first separately dissolved in DMSO. The combination of the two solutions results in the fast precipitation of a white solid. Scanning electron microscopy (SEM) investigation at lower magnification (**Figure 1**a) shows that the white precipitate is composed of spheres with an average diameter of around 2–3 µm and a narrow size distribution. Higher magnification image (Figure 1b) reveals that the spherical particles are composed of 3D plates with thickness of 30–50 nm, showing the evidence of hexagonal symmetry. The formation of these plates can be directly related to the structure of the molecular assembly of MCA as shown in **Scheme 1**.

Figure S1 (Supporting Information) shows an X-ray diffraction pattern of MCA. Three well-resolved peaks at lower angles, 10.67, 18.48, and 21.41°, can be indexed as (100), (110), and (200), respectively, supporting the in-plane hexagonal pattern of

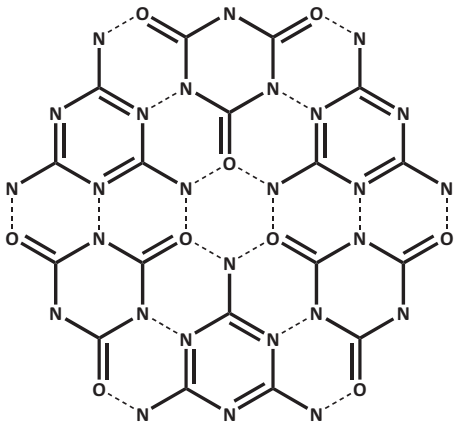

Scheme 1. Chemical formula of melamine-cyanuric acid hydrogen bonded aggregates (MCA). Dotted lines indicate hydrogen bonds.

channels. We attribute an intense peak at 27.9° and a d-spacing of 0.320 nm to graphite-like stacking of individual 2D sheets. MCA is further evidenced by Fourier transform infrared (FT-IR) analysis (Supporting Information Figure S2). It has been reported that hydrogen bonding of N–H…O and N–H…N linkages between melamine and cyanuric acid result in a shift of the C=O stretching vibration of cyanuric acid to a higher frequency and the triazine ring vibration of melamine to a lower frequency.[11] Indeed, we found that the vibrational spectra shows that the C=O stretching vibration of cyanuric acid at 1693 and 1754 cm^{-1} is shifted to 1732 and 1779 cm^{-1}, while the triazine ring vibration of melamine moves from 808 cm^{-1} to 765 cm^{-1}.

2.2. Thermal Polycondensation of MCA to MCA-CN

In order to create the desired carbon nitride based photocatalyst, MCA was heated to different temperatures. When melamine is solely used as a carbon nitride precursor, it is known that different intermediate products are created during heating.[12] Thus, melamine forms a tri-*s*-triazine monomer, called melem at temperatures around 380 °C. Further heating then causes polymerization of melem first into a linear polymer, melon, at around 450 °C, which then can further condense to yield an ill-defined, 2D carbon nitride in the temperature range of 450–600 °C. Thermal decomposition of this carbon nitride occurs at ≈650 °C in any atmosphere. It should be noted that it has been shown by Schnick et al. that the thermal polycondensation process of melamine proceeds not much further than to the polymeric compound, melon.[13]

At temperatures above 325 °C, cyanuric acid reacts with ammonia to give ammelide, ammeline, and finally melamine.[14] Since ammonia is produced during the condensation of melamine, heating of the precipitate under a protective gas can be expected to finally yield the carbon nitride, comparable to the materials produced from pure melamine. The products after polycondensation indeed showed the typical yellow colour of g-CN. The photocatalytic activity of bulk g-CN synthesized from conventional molecular precursors correlates with the degree

of polycondensation and thus the formation of electronic band structure appropriate for the target reaction. We, therefore, performed careful analysis of chemical, texture, optical, and electronic properties of the resulting material by using FT-IR, X-ray diffraction, electron microscopy, NMR spectroscopy, elemental analysis (EA), X-ray photoelectron spectroscopy (XPS), UV-visible diffuse reflectance spectroscopy (UV-vis DRS), electrochemical impedance spectroscopy (EIS) and time-resolved fluorescence spectroscopy.

2.2.1. Chemical Structure and Texture of MCA-CN

FT-IR spectra (Supporting Information Figure S3) indicate that the functionalities of melamine and cyanuric acid are retained up to 350 °C. At 400 °C, the characteristic peaks of melamine and cyanuric acid disappear and new peaks showing the formation of tri-*s*-triazine arise at 810, 1313, 1415, 1599, and 3200 cm^{-1}.[12] Further condensation at higher temperatures increases the intensity of these peaks. At 550 °C, the resulting material shows three major peaks centred at 3500–3000, 1800–1100, and 800 cm^{-1}, proving the presence of a heterocyclic ring structure and amine functionalities.

X-ray diffraction (XRD) patterns of MCA heated to different temperatures (Supporting Information Figure S4) show first an increase in intensity of the peaks observed for MCA. The defined structure, however, disappeared at 400 °C as seen from IR results and a broad peak, indexed as (002) and indicating a distance of 0.327 nm, is observed at 550 °C. The interlayer distance between 2D sheets was kept constant (Δd_{002}<0.01 nm) during the further heat treatment to 550 °C. The condensation, therefore, progressed mainly inside the 2D sheets without changing the overall stacking structure. The intralayer periodicity at 13.2°, corresponding to a distance of 0.67 nm and indexed as (100), results from the trigonal nitrogen linkage of tri-*s*-triazine units at around 450 °C, which is very early in the condensation process compared to other molecular precursors.[15] It has been shown that the polycondensation process strongly depends on the molecular precursor. For example, dicyandiamide retards the easy sublimation of melamine by forming the H-bridge with intermediate melamine.[3] The presence of additional leaving motifs like oxygen and sulfur in urea, thiourea, and trithiocyanuric acid facilitates the condensation process and enables structural perfection.[15b,c] The oxygen containing intermolecular structure connected by hydrogen bonding and stacked in graphitic fashion, i.e., MCA, features all of these characteristics resulting in the early condensation. Compared to that of bulk g-CN synthesized from dicyandiamide at 550 °C (DCDA-CN), it was found that the interlayer distance was shifted to lower value while that of (100) peak maintained unchanged, indicating the formation of a more condensed g-CN. The (002) peak became less pronounced and broad at above 500 °C. We attribute this to the formation of thin nanosheets structure.

Further structural analyses were performed by solid state ^{13}C CP/TOSS NMR and N 1s XPS, and confirmed the presence of tri-*s*-triazine units connected by trigonal nitrogen in MCA heated at 550 °C. Two chemical shifts were observed at 156.6 and 164.3 ppm in the NMR spectra (Supporting Information Figure S5). These are assigned to C–N_3 and C–N–$H_{(2)}$ in tri-*s*-triazine, respectively.[12] Deconvolution of N 1s XPS spectrum distinguishes the signals centred at 399.0, 400.3, and 401.5 eV corresponding to C–N=C, N–C_3, and C–N–$H_{(2)}$ coordination, respectively (Supporting Information Figure S6).[16] The peak area of tertiary nitrogen surpasses that of the hydrogen containing amino functions by a factor of 3.9. This value is comparable to that (3.9) of bulk carbon nitrides synthesized from dicyandiamide (DCDA-CN) at 550 °C and is higher than that (2.8) obtained from the thermal reaction of melamine at 550 °C (data not shown). Elemental analyses gave a C/N ratio of 0.72 and a hydrogen content of 1.93 wt%. It can be concluded from these results that the condensation of MCA at 550 °C forms a carbon nitride based on tri-*s*-triazine units (MCA-CN) and that the degree of condensation is comparable to that of DCDA-CN without using inorganic hard template.[3]

SEM images show the evolution of the microstructure in MCA during heat treatment (**Figure 2**). While MCA is made up of individual platelets, these platelets are merged into larger crystals at 350 °C. The hexagonal unit cell with 120° angles can be easily identified by X-ray diffraction studies of these crystals. However, no crystalline structures can be observed in the material at 400 °C, yielding a more polymer-like, i.e., amorphous appearance. The accompanied substance and mass loss during condensation results in large voids in MCA, yielding carbon nitride hollow spheres, which collapse to some extent at higher temperatures. While the pristine layered structure of 3D plates is followed by the formation of MCA-CN, the radius of the spheres decreases to ≈60% in the lateral direction and to ≈30% in the longitudinal direction at 550 °C to give an oblate spheroid.

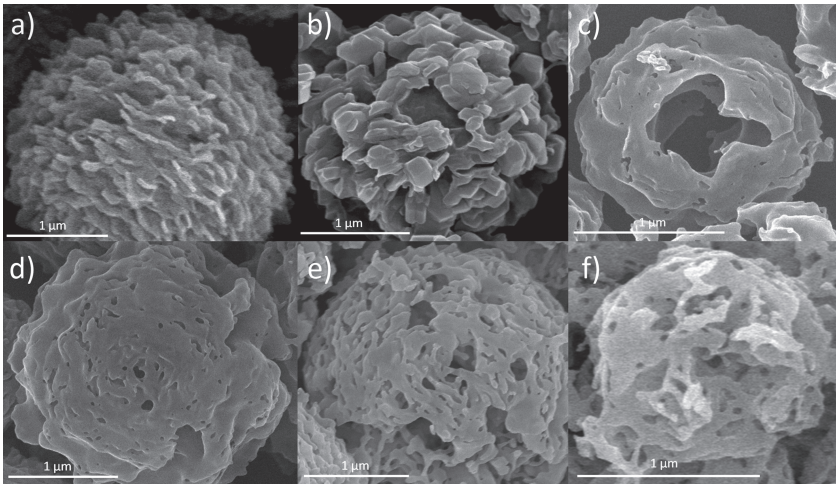

Figure 2. SEM images of MCA heated at different temperatures;:a) as-synthesized and heated at b) 350, c) 400, d) 450, e) 500, and f) 550 °C.

Nitrogen sorption analysis indicates that mesopores of about 4 and 36 nm are generated at 400 °C where MCA has a BET surface area of 77 $m^2 g^{-1}$ and a pore volume of 0.4 $cm^3 g^{-1}$ (Supporting Information Figure S7 and

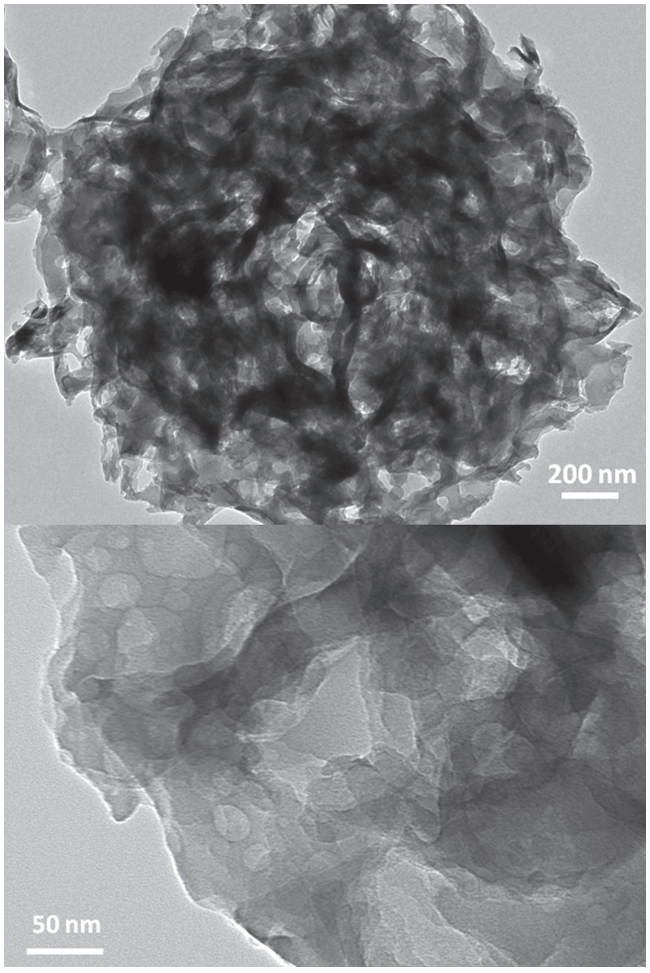

Figure 3. TEM images of MCA heated at 550 °C.

Table S1). The population of larger pores rapidly decreases at 450 °C due to structure shrinkage. The resulting MCA-CN has a BET surface area of 51 m^2 g^{-1} and a pore volume of 0.1 cm^3 g^{-1}. TEM images (**Figure 3**) showed that the 30–40 nm pores are embedded in the nanosheet structure of MCA-CN.

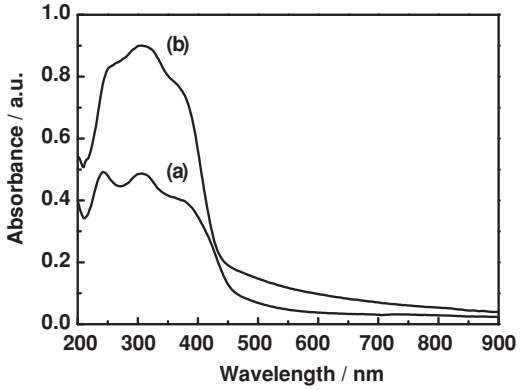

Figure 4. Diffuse reflectance absorption spectra of a) DCDA and b) MCA heated at 550 °C.

2.2.2. Electronic Band Structure and Photophysical Behavior of Charge Carriers in MCA-CN

UV-vis diffuse reflectance spectrum of MCA-CN features typical semiconductor-like absorption (**Figure 4**). It has a band edge at ca. 450 nm corresponding to 2.76 eV, indicating slight blue shift by 0.16 eV compared to DCDA-CN. This reflects the quantum confinement effects of the thermally induced thinner (or smaller) nanosheet structure as is evidenced in SEM/TEM analysis. The hypsochromic shift induced by H-aggregates formation during the high temperature polycondensation procedure is also partially responsible. MCA-CN shows stronger absorption intensities compared to DCDA-CN under both ultraviolet and visible light extending to 750 nm. It is believed that the enhanced optical absorption property of MCA-CN results mainly from the multiple reflection of incident light in the mesoporous hollow spheres and within the layered structure of the carbon nitride wall.[17]

The electronic band structure of MCA-CN can be examined in detail by EIS analysis and Mott-Schottky relationship. The apparent capacitance is measured as a function of potential at frequency ranges on the order of kHz. The flat band potential can be determined as an x-intercept in the Mott-Schottky plot (**Figure 5**a). The positive slope of Mott-Schottky plot reveals n-type semiconductor characteristics of MCA-CN. The flat band

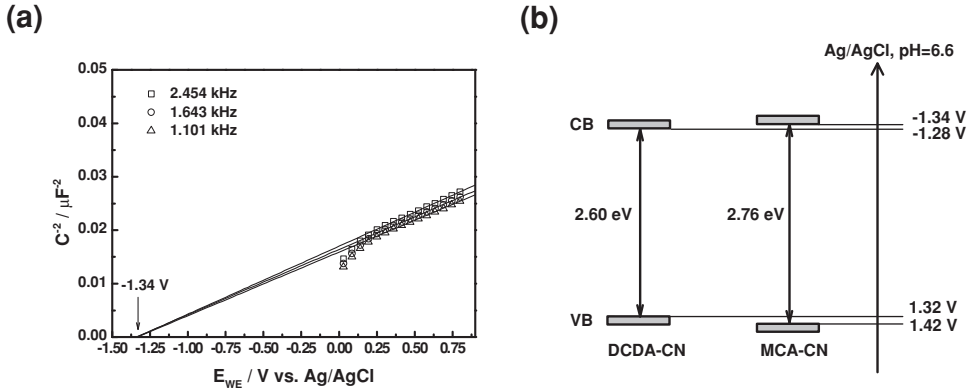

Figure 5. a) Mott-Schottky plot and b) schematic diagram of electronic band structure of DCDA-CN and MCA-CN.

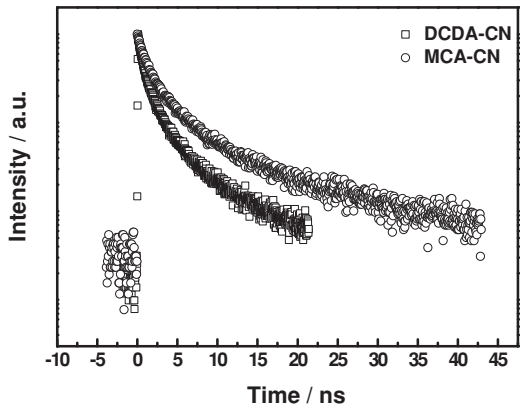

Figure 6. Time-resolved fluorescence decay spectra of DCDA-CN and MCA-CN monitored at 480 nm by time-correlated single-photon counting. The samples were excited by the incident light of 400 nm from a picosecond pulsed light-emitting diode.

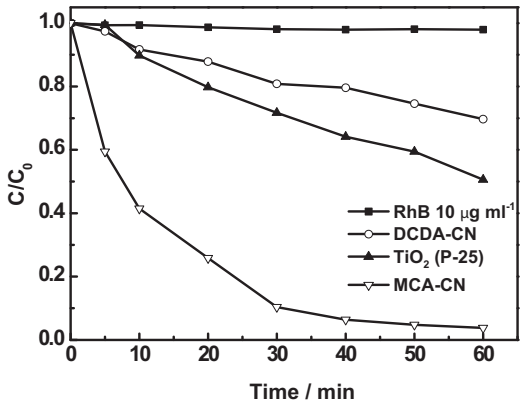

Figure 7. Concentration changes of RhB as a function of irradiation time with different catalyst under visible light irradiation. C_0 = 10 μg mL^{-1}.

potential of MCA-CN in aqueous solution at pH 6.6 was calculated as −1.34 V vs. Ag/AgCl. The electronic band structure of MCA-CN is thus determined with the band gap as shown in Figure 5b. Both the conduction and valence band edges shift to more negative and positive values, respectively, than those of DCDA-CN. This again proves that the nanosheet is thin enough that the quantum confinement effects dominate. Further, it is expected that the electronic band structure of MCA-CN with higher energy level would possess the thermodynamically enhanced reduction and oxidation power in photocatalytic reactions. The charge-transfer rate between semiconductor catalyst and redox species in solution also depends on such energy level correlation.[18]

The recombination kinetics of photoexcited charge carriers in MCA-CN was observed by time-resolved fluorescence spectroscopy. The fluorescence intensity at 480 nm was monitored upon excitation at 400 nm. The decay spectra of DCDA-CN and MCA-CN are shown in **Figure 6**. The presence of multi-exponential decays is evident from the curvature in the plot of Log intensity versus time. The spectra are well fit to double-exponential decay model. The lifetime and its fractional contribution are obtained from nonlinear least squares analysis and summarized in Supporting Information Table S2. Prolonged lifetimes clearly indicate that the recombination of photoexcited carriers is greatly suppressed in MCA-CN. The carriers are survived twice as long as those of DCDA-CN while maintaining the fractional contribution of each lifetime. The longer (5.456 ns) and shorter (1.027 ns) lifetime have the fractional contribution of 72% and 28%, respectively, on the total fluorescence intensity. We believe that such prolonged lifetime originates from the high degree of polycondensation in which the electron-hole recombination is inhibited due to the less density of defects. The thin nanosheet structure would also possess higher electrical conductivity, facilitating migration of the carriers to the surface redox species.

2.3. Evaluation of Photocatalytic Activity of MCA-CN in RhB Degradation

In order to demonstrate the structure-function correction of MCA-CN, we evaluated photodegradation of RhB as a function of time under visible light irradiation (**Figure 7**). Visible light irradiation does not cause degradation of RhB in the absence of a photocatalyst. 30% and 50% degradation of RhB was observed in the presence of DCDA-CN and P-25 (Degussa, TiO_2), respectively. The decreased concentration of RhB by P-25 is due to the self-sensitization-induced degradation of RhB, as TiO_2 only works under UV light. On the other hand, MCA-CN was able to completely degrade RhB in 1 h irradiation with about 60% of the RhB being initially degraded in 10 min. This greatly enhanced degradation capability of MCA-CN was maintained without a significant decrease in efficiency when the photocatalytic reaction was repeated (**Figure 8**). A control experiment under dark condition indicates that 27% of RhB is removed from the aqueous solution by adsorption onto MCA-CN in 10 min, leading to an initial (or overall) high activity for photodegradation of RhB (Supporting Information Figure S8). The k value indicating activity of a photocatalyst is 0.062 for MCA-CN which is almost 10 and 6 times larger than that for DCDA-CN and P-25, respectively (Supporting Information Figure S9).

UV-vis spectra of degraded RhB reveal that photocatalytic degradation of RhB by MCA-CN is dominated by two different mechanisms, 1) direct degradation and 2) de-ethylation of RhB.[19] The absorption spectra of RhB is initially centered at 554 nm corresponding to *N,N,N′,N′*-tetraethylrhodamine,

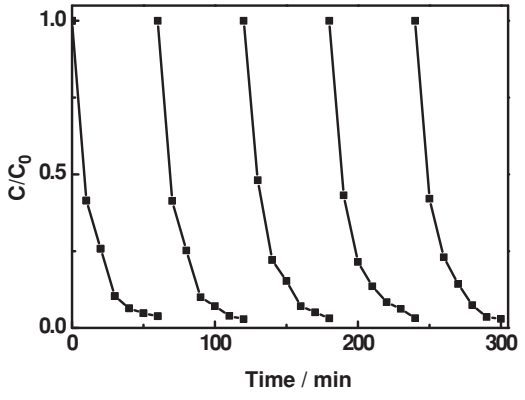

Figure 8. Cycling runs of RhB degradation in MCA-CN under visible light irradiation. C_0 = 10 μg mL^{-1}.

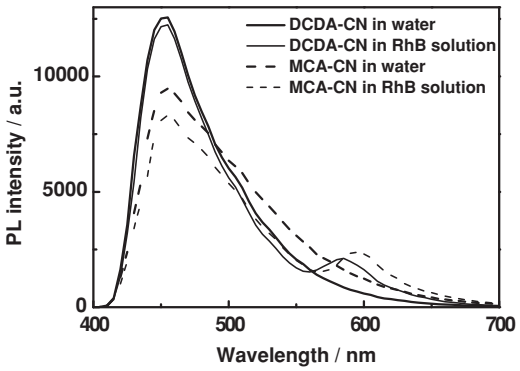

Figure 9. PL spectra of DCDA- and MCA-CN in water or RhB solution. Excitation at 375 nm.

and then shifts to 498 nm which we attribute to rhodamine, proving that de-ethylation of RhB became dominant in the latter stage (Supporting Information Figure S10). Considering the electronic band structure for MCA-CN, the reactive oxidation species for photocatalytic reaction are mainly the superoxide radicals formed by photogenerated electrons of MCA-CN. It is known that the hydroxyl radicals are also generated by the photogenerated electron induced multistep reduction of O_2 ($O_2 + e \rightarrow O_2\cdot$, $O_2\cdot + e + 2H^+ \rightarrow H_2O_2$, $H_2O_2 + e \rightarrow \cdot OH + OH^-$).[20] Supporting Information Table S3 shows that the photodegradation efficiency of RhB is slightly increased when 0.1 mM H_2O_2 is added into carbon nitride photocatalysis system. The introduced H_2O_2 accelerates the reaction of $H_2O_2 + e^- \rightarrow \cdot OH + OH^-$ and improves the photocatalytic degradation efficiency.[21] The photoluminescence (PL) spectra of photocatalyst suspension in distilled water and RhB (10 μg mL^{-1}) are shown in **Figure 9**. Upon photoexcitation at 375 nm, g-CNs exhibit a PL peak at 455 nm. It is notable that the PL intensity of MCA-CN suspension in RhB solution is slightly lower than that in distilled water, whereas DCDA-CN shows the little difference. This means that the recombination process of photogenerated electron-hole pairs is partially prevented by RhB probably due to the direct oxidation of RhB by the photogenerated holes in the valence band of MCA-CN, again proving the enhanced photooxidation ability of MCA-CN resulted from the quantum confinement effect and H-aggregates formation.[22]

3. Conclusions

In conclusion, we have demonstrated that the molecular cooperative assembly between melamine and cyanuric acid, MCA, is a promising precursor material of g-CN enabling simultaneous optimization of the texture and photoelectric properties. The preformed flower-like, layered spherical structure is successfully incorporated into the subsequently formed g-CN. The oxygen containing intermolecular structure connected by hydrogen bonding and stacked in graphitic fashion facilitates the condensation process and enables the structural perfection. The resulting MCA-CN, therefore, induces stronger optical absorption, widens the bandgap, and increases the lifetime of photoexcited charge carriers compared to that of DCDA-CN, while maintaining the chemical structure similar to that of DCDA-CN without using hard template. Finally, the photocatalytic activity of MCA-CN was greatly enhanced in photodegradation of RhB without the aid of co-factors, such as H_2O_2 and metal ions. Current research focuses on the formation of various molecular cooperative assembly depending on the precursor molecules, solvent type, and synthesis temperature and its effect on the texture and photoelectric properties of the resulting g-CN.

4. Experimental Section

Synthesis of MCA-CN: Microsized mesoporous carbon nitride hollow spheres were synthesized by using 1:1 hydrogen-bonded melamine-cyanuric acid network. Due to the limited solubility of them in normal solvent, DMSO was utilized as a solvent to dissolve melamine and cyanuric acid. In a typical synthesis, 0.5 g of melamine and 0.51 g of cyanuric acid were dissolved in 20 mL and 10 mL of DMSO, respectively, with sonication. After complete dissolution, both solutions were kept at room temperature and then mixed together for 10 min to give white precipitates. Subsequently, the mixture was filtered and washed with ethanol. Resulting white powder was dried at 50 °C and calcined at 550 °C for 4 h with the heating rate of 2.3 °C min^{-1} under nitrogen.

Characterization: SEM/TEM images were taken with Hitachi S4800 and JEOL FB-2100F (HR) at an acceleration voltage of 200 kV, respectively. Characterization by XRD was carried out in reflection mode (Cu Kα radiation) on a Rigaku D/MAX-2500 diffractometer. Elemental analysis was performed using a Vario EL 3 elemental analyzer manufactured by Elementar. The adsorption/desorption isotherms of nitrogen at –196 °C were measured using a Micromeritics ASAP 2020. The Brunauer-Emmett-Teller (BET) equation was used to calculate the apparent surface area from adsorption data obtained at P/P_0 between 0.05 and 0.2. The total volume of the mesopores was calculated from the amount of nitrogen adsorbed at $P/P_0 = 0.99$, assuming that adsorption on the external surface was negligible compared to adsorption in pores. Pore size distribution was evaluated by BJH method using desorption branch. FT-IR spectra were collected on a JASCO FT-IR 470 plus with the average of 12 scans with a resolution of 4 cm^{-1} from 4000 cm^{-1} to 600 cm^{-1}. ^{13}C CP/TOSS (CP/MAS with side band suppression) NMR spectra were collected on a solid-state FT-NMR spectrometer (Bruker, DSX 400 MHz) with a 7 mm MAS probe. Spin speed of 6.5 kHz and an initial contact time of 3 ms before inverting the sign of the ^1H radiation were used. The signals were referenced to adamantane. XPS spectra were provided by ESCALAB250. Optical absorbance spectra were examined by ultraviolet diffuse reflectance spectroscopy (V670-Jasco, Japan). Time-resolved fluorescence spectroscopy was recorded at room temperature by Hamamatsu R928 photomultiplier tube. EIS analysis was performed using Bio-Logic VMP3 potentiostat. g-CN electrode was prepared by spreading aqueous slurries of g-CN over FTO glass substrate. The suspension was prepared by dispersing 50 mg of g-CN with 200 μL of H_2O, 5 μL of acetylacetone, and 5 μL of Triton X-100. The film was annealed at 350 °C for 2 h under air.

Photocatalytic Activity Test: RhB was chosen as the degrading pollutions to test photocatalytic activities of MCA-CN and DCDA-CN. The light irradiation system contains a 1 kW Hg lamp with cut-off filter ($\lambda > 420$ nm). To evaluate photocatalytic activities of carbon nitrides, 1 mg of carbon nitride was mixed with 1 mL of RhB solution (10 μg mL^{-1}) in distilled water under photoirradiation. The degradation efficiencies of RhB were evaluated using UV-vis absorption spectra to measure the concentration of remained RhB in solution. The concentration changes are described by C/C_0, where C_0 is the initial concentration of RhB and C is the remained concentration of RhB. The concentration of RhB is calculated by a calibration curve which is measured at 554 nm of UV-vis absorption spectra. All PL spectra were measured by microplate spectrofluorometer (Gemini EM-Molecular Devices, USA).

Supporting Information

Supporting Information is available from the Wiley Online Library or from the author.

Acknowledgements

This work was supported by the Project "Light2Hydrogen" of the BMBF (03IS2071D), KBSI grant T31605 to S.-G.L, Brain Korea 21 (BK21), the Advanced Biomass R&D Center (ABC-2011-0031354) of Global Frontier Project funded by the Ministry of Education, Science, and Tech-nology of Korea and by the University of California Lab Fees Research Program.

Received: December 17, 2012
Revised: January 11, 2013
Published online: February 26, 2013

[1] G. M. Whitesides, J. P. Mathias, C. T. Seto, *Science* **1991**, *254*, 1312.
[2] a) C. T. Seto, G. M. Whitesides, *J. Am. Chem. Soc.* **1990**, *112*, 6409; b) C. T. Seto, G. M. Whitesides, *J. Am. Chem. Soc.* **1993**, *115*, 905; c) A. Ranganathan, V. R. Pedireddi, C. N. R. Rao, *J. Am. Chem. Soc.* **1999**, *121*, 1752.
[3] A. Thomas, A. Fischer, F. Goettmann, M. Antonietti, J. O. Muller, R. Schlogl, J. M. Carlsson, *J. Mater. Chem.* **2008**, *18*, 4893.
[4] F. Goettmann, A. Fischer, M. Antonietti, A. Thomas, *Angew Chem. Int. Ed.* **2006**, *45*, 4467.
[5] X. F. Chen, Y. S. Jun, K. Takanabe, K. Maeda, K. Domen, X. Z. Fu, M. Antonietti, X. C. Wang, *Chem. Mater.* **2009**, *21*, 4093.
[6] a) X. F. Chen, J. S. Zhang, X. Z. Fu, M. Antonietti, X. C. Wang, *J. Am. Chem. Soc.* **2009**, *131*, 11658; b) X. C. Wang, K. Maeda, X. F. Chen, K. Takanabe, K. Domen, Y. D. Hou, X. Z. Fu, M. Antonietti, *J. Am. Chem. Soc.* **2009**, *131*, 1680; c) K. Maeda, X. C. Wang, Y. Nishihara, D. L. Lu, M. Antonietti, K. Domen, *J. Phys. Chem. C* **2009**, *113*, 4940; d) S. C. Yan, Z. S. Li, Z. G. Zou, *Langmuir* **2009**, *25*, 10397; e) K. Kailasam, J. D. Epping, A. Thomas, S. Losse, H. Junge, *Energy Environ. Sci.* **2011**, *4*, 4668.
[7] X. C. Wang, K. Maeda, A. Thomas, K. Takanabe, G. Xin, J. M. Carlsson, K. Domen, M. Antonietti, *Nat. Mater.* **2009**, *8*, 76.
[8] a) A. Fischer, M. Antonietti, A. Thomas, *Adv. Mater.* **2007**, *19*, 264; b) A. Fischer, J. O. Muller, M. Antonietti, A. Thomas, *ACS Nano* **2008**, *2*, 2489; c) Y. S. Jun, W. H. Hong, M. Antonietti, A. Thomas, *Adv. Mater.* **2009**, *21*, 4270.
[9] A. Thomas, F. Goettmann, M. Antonietti, *Chem. Mater.* **2008**, *20*, 738.
[10] J. S. Zhang, X. F. Chen, K. Takanabe, K. Maeda, K. Domen, J. D. Epping, X. Z. Fu, M. Antonietti, X. C. Wang, *Angew. Chem. Int. Ed.* **2010**, *49*, 441.
[11] G. Arrachart, C. Carcel, P. Trens, J. J. E. Moreau, M. W. C. Man, *Chem. Eur. J.* **2009**, *15*, 6279.
[12] B. Jurgens, E. Irran, J. Senker, P. Kroll, H. Muller, W. Schnick, *J. Am. Chem. Soc.* **2003**, *125*, 10288.
[13] B. V. Lotsch, M. Doblinger, J. Sehnert, L. Seyfarth, J. Senker, O. Oeckler, W. Schnick, *Chem. Eur. J.* **2007**, *13*, 4969.
[14] P. M. Schaber, J. Colson, S. Higgins, E. Dietz, D. Thielen, B. Anspach, J. Brauer, *Am. Lab.* **1999**, *31*, 13.
[15] a) M. J. Bojdys, J. O. Muller, M. Antonietti, A. Thomas, *Chem. Eur. J.* **2008**, *14*, 8177; b) J. S. Zhang, J. H. Sun, K. Maeda, K. Domen, P. Liu, M. Antonietti, X. Z. Fu, X. C. Wang, *Energy Environ. Sci.* **2011**, *4*, 675; c) G. G. Zhang, J. S. Zhang, M. W. Zhang, X. C. Wang, *J. Mater. Chem.* **2012**, *22*, 8083.
[16] E. Z. Lee, Y. S. Jun, W. H. Hong, A. Thomas, M. M. Jin, *Angew. Chem. Int. Ed.* **2010**, *49*, 9706.
[17] a) H. X. Li, Z. F. Bian, J. Zhu, D. Q. Zhang, G. S. Li, Y. N. Huo, H. Li, Y. F. Lu, *J. Am. Chem. Soc.* **2007**, *129*, 8406; b) J. S. Zhang, J. H. Sun, K. Maeda, K. Domen, P. Liu, M. Antonietti, X. Z. Fu, X. C. Wang, *Energy Environ. Sci.* **2011**, *4*, 675.
[18] T. Inoue, A. Fujishima, S. Konishi, K. Honda, *Nature* **1979**, *277*, 637.
[19] Y. Cui, Z. Ding, P. Liu, M. Antonietti, X. Fu, X. Wang, *Phys. Chem. Chem. Phys.* **2012**, *14*, 1455.
[20] G. M. Liu, X. Z. Li, J. C. Zhao, S. Horikoshi, H. Hidaka, *J. Mol. Catal. A: Chem.* **2000**, *153*, 221.
[21] T. X. Wu, G. M. Liu, J. C. Zhao, H. Hidaka, N. Serpone, *J. Phys. Chem. B* **1998**, *102*, 5845.
[22] S. C. Yan, Z. S. Li, Z. G. Zou, *Langmuir* **2010**, *26*, 3894.